Hindawi
Advances in Civil Engineering
Volume 2023, Article ID 9997061, 14 pages
https://doi.org/10.1155/2023/9997061

*Research Article*

# Exploratory Field and Laboratory Investigation on the Use of Noncontact Digital Ski Sensor in the South Korea Expressway Network

**In Bae Kim,[1,2] Ki Hoon Moon ,[2] and Augusto Cannone Falchetto [3]**

[1]*School of Civil, Environmental and Architectural Engineering, Korea University, 145 Anam-ro Seongbukgu, Seoul 02841, Republic of Korea*
[2]*Research Strategy & Planning Department, Korea Expressway Corporation, Dongtan-myeon Hwaseong-si, Gyeonggi-do 445-812, Republic of Korea*
[3]*Department of Civil Engineering, Aalto University, Rakentajanaukio 4, Espoo 02150, Finland*

Correspondence should be addressed to Ki Hoon Moon; goufcustom@naver.com

Received 12 January 2023; Revised 14 May 2023; Accepted 29 July 2023; Published 17 October 2023

Academic Editor: Okan Sirin



In the case of asphalt pavement construction, better smoothing and reliable material performance acquisition are essential. In South Korea, the next-generation asphalt pavement-smoothing technology, known as the noncontact digital ski (NCDS), started to be used in expressway construction in 2018, making this system an essential tool in the paving industry. The present work thoroughly assessed how employing the NCDS system affected the response of the pavement material at low temperatures. Portions of paved roads with and without NCDS were assessed for the international roughness index (IRI, m/km). The development of thermal stress propagation was then examined using the bending beam rheometer on asphalt samples from the road. Based on straightforward visual and statistical analysis, it was discovered that using NCDS produces significantly lower IRI and reduced thermal stress, which raises the possibility that using NCDS has the potential for better low-temperatures predictions.

## 1. Introduction

For road users to enjoy a satisfying driving experience, good road condition is essential [1–8]. Smooth and flat road surfaces are advantageous since they lead to lower energy consumption and minimize maintenance and emissions [4–6]. Also, a smoother and even asphalt pavement surface may be safer, reducing the accident rate and consequent social costs. In addition, this can result in an infrastructure that is less prone to distress, which leads to higher costs due to more frequent maintenance activity throughout the pavement service life [2, 5, 6, 8–13].

The smoothness of a road is frequently assessed using the international roughness index (IRI, m/km) as operated by many pavement management agencies [4–6, 14, 15]. The IRI provides crucial information on pavement roughness; this parameter is conventionally derived based on the pavement profile measurements and mathematically schematized as a quarter-car vehicle with a simulated constant vehicle speed of 80 km/hr [16–18]. Higher IRI values indicate poor and negative pavement smoothness; therefore, specific limiting thresholds are set and then defined in many pavement agencies. For the expressway system (South Korea's primary highway network), for instance, an IRI of 1.6 m/km is necessary for the quality control process [19, 20]. Different research has investigated pavement smoothness by investigating newer material solutions, improved pavement structure, and specific construction strategies [4–6, 21–24]. More sophisticated research was devoted to studying computational solutions for estimating and predicting pavement smoothness [8, 9, 14, 25–28], leaving little and less attention to the construction practice and technical solutions, which may ultimately result in better surface characteristics. Such a limited interest in the innovation and development of asphalt paving technology (e.g., paving equipment) for improving smoothness can be partially associated with a poor understanding and communication

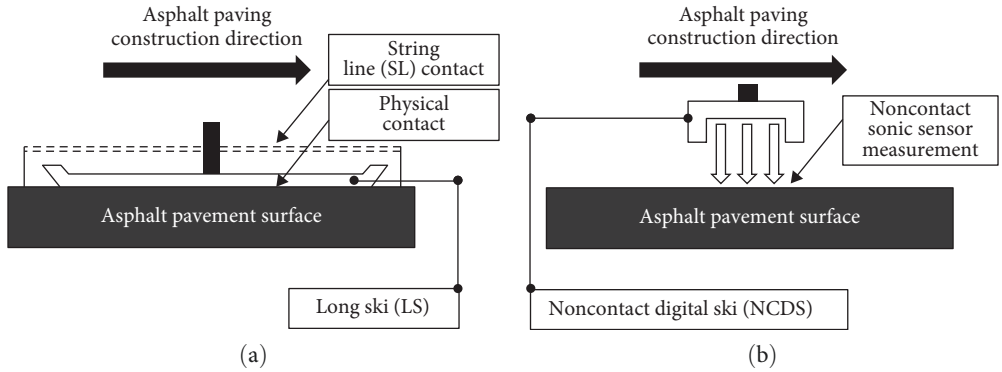


Figure 1: (a) LS (long ski) + SL (string line) and (b) NCDS (noncontact digital ski) systems.

between academia and the asphalt pavement construction industry. Beyond the research environment, contractors recognized the necessity for more advanced tools as a critical component in enhancing infrastructure quality [4–6]. The long-range surface contact ski (LSCS) system, also identified as long ski (LS), is commonly combined with the string line (SL) to define the smoothness in Korean Expressway construction and many other Asian countries [4–6]. However, this system presents limitations that constrain further pavement surface improvement (e.g., resulting in lower IRI) [4–6]. Many machine industries developed novel and advanced devices that may enable better surface smoothness of asphalt pavements. Multisonic sensors provide a solid alternative as they rely on the acoustic emissions [29–32] resulting in the noncontact digital ski (NCDS) system for asphalt pavement applications [31, 32]. Contrary to earlier traditional approaches, the NCDS does not call for direct physical contact between the machine and the road surface. A noncontact distance measuring technique that uses readings from several sensors automatically determines the design thickness of the layer to be paved [4–6, 30–32].

In comparison to the traditional pavement surface smoothing technique (e.g., LS: long ski + SL: string line), the NCDS system, based on this technology, may be able to deliver consistent and enhanced pavement smoothness, also for curved sections and long ranges. Figure 1 schematizes how the LS + SL and NCDS systems vary from one another.

## 2. Methodology

This study compares the typical South Korean approach of combining the LS and SL techniques (LS + SL) for building composite pavement in the expressway network with the impact of using NCDS for increasing road smoothness [15–17]. The IRI values from the LS + SL and NCDS were visually and statistically analyzed. In order to assess the cracking resistance of asphalt mixture at low temperatures, bending beam rheometer (BBR) was used to carry out creep test field material from sections paved with the NCDS and LS + SL methods [33–38]. In assessing asphalt material low-temperature performance evaluation, indirect test (IDT), semicircular bending (SCB), or dynamic modulus (DM) tests were widely used [36, 39–41]. One of the drawbacks of these testing methods is associated with the expensive cost of the testing device and the large testing size of the specimens making the field testing cores obtained from thin surface layers hard to perform. Several studies experimentally demonstrated that the BBR mixture creep test can provide good estimation of the low-temperature response of paving mixtures as the conventional IDT testing approach [35–37] with an inexpensive sample preparation procedure, lower testing device costs, and the same sample size used to binder testing [33, 36, 42]. The BBR creep test was thus used for this work. A visual and statistical evaluation was used analogously to the one adopted for the IRI data. The key findings and conclusion are then discussed. Figure 2 illustrates the adopted methodology.

## 3. Background Information

*3.1. String Line (SL): Surface Smoothing Method Based on Physical Contact.* The string line method consists of positioning steel sticks every 5–10 m on the ground along the road that will be covered with asphalt. After that, a steel wire is continually attached to the already-installed steel sticks and connected to them. The goal pavement thickness is defined by the level supplied by the steel line. If no significant roughness or fluctuations in the evenness of the ground or underlying pavement layer are present, the asphalt paving machine continuously discharges asphalt materials based on the preinstalled steel line. The string line method is widely adopted in the pavement industry due to its simplicity and reasonable smoothness quality that is achievable during construction (both for county road and expressway construction) [4–6, 23]. Nevertheless, this approach presents a series of limitations associated with the high-labor-intensive procedures that demand significantly skilled workers. Therefore, theLS equipment is used in conjunction with the SL. An example of an SL system adopted in a pavement construction site on the Korean expressway network is shown in Figure 3.

*3.2. Long-Ski (LS): Surface Smoothing Method Based on Physical Contact.* In this method, to further enhance the pavement smoothness, a series of steel plates/rollers were in contact with the paving surface. A single beam that was between 10 and 15 m long and resembling a long ski was created by the connecting plates or rollers. For this peculiar characteristic, this smoothing

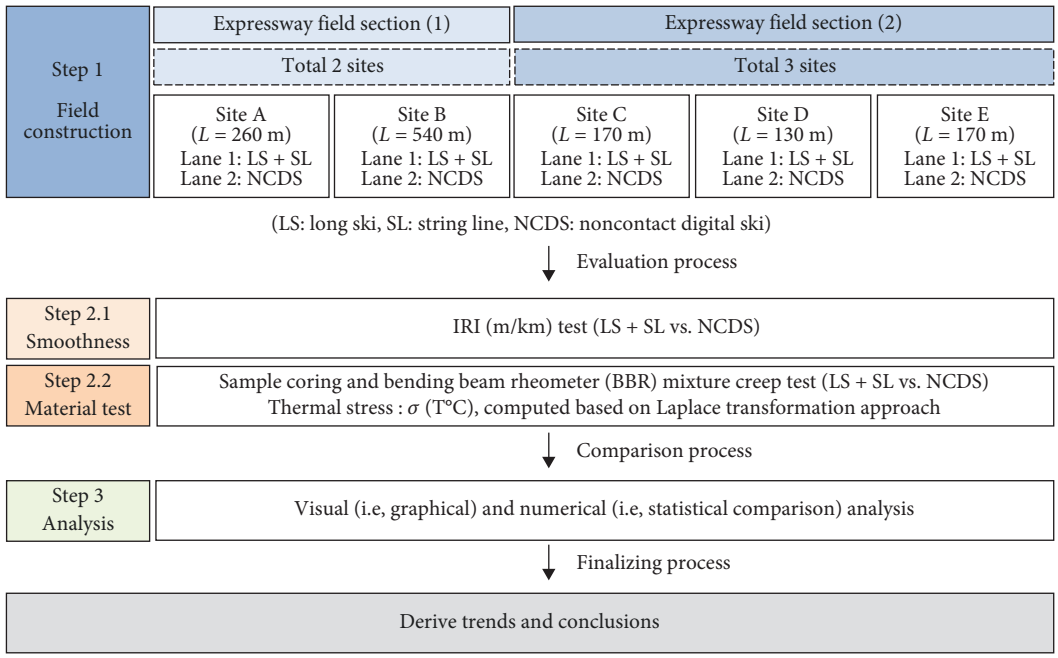


Figure 2: Methodology.


Figure 3: String-line (SL) system on a Korean expressway (Chuncheon-Yang Yang Highway, South Korea).

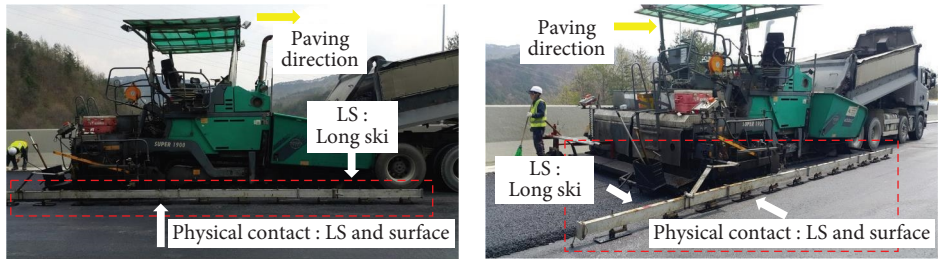


Figure 4: Long-ski (LS) system on a Korean expressway—Chuncheon-Yang Yang Highway, South Korea.

solution is known as LSCS or, in short, LS. Similar to the SL method, the LS approach provides a simple tool to achieve a satisfactory smoothing of the asphalt pavement. This solution is coupled with moderately limited operation costs compared to other methods, such as sonic sensors. Two significant limits may be found, though. The smoothness of the final surface layer may be severely impacted by irregularities on the existing surface since this technology first requires a lower reference surface where the asphalt material will be laid. Second, the LS method presents limited flexibility when a curved section needs to be paved. Figure 4 illustrates an example of an LS paving system. Therefore, advanced and more flexible techniques are required to enhance the degree of pavement smoothness.

*3.3. Noncontact Digital Ski (NCDS): Surface Smoothing Method Based on Nonphysical Contact.* The NCDS apparatus uses 3–4 sets of multisonic sensors (also known as cartridges) that were each attached to a long beam that were typically

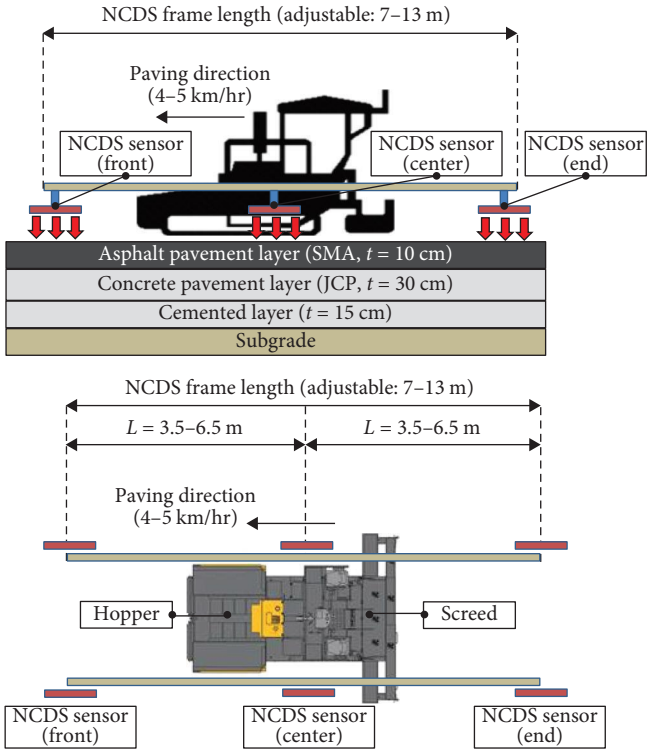


Figure 5: Basic concept of noncontact digital ski (NCDS) system.

between 7 and 13 m long. Five separate, acoustic emission-based sensors make up each multisonic sensor cartridge. An enormous beam with several multisensor cartridges was fastened to one side of the asphalt paver during pavement building. The NCDS system was installed on both sides of the asphalt paver when improved pavement smoothness is desired. With three or four sensor arrays, each thickness measurement offered 15–20 single data points on either side of the asphalt paver. Out of this data set, each cartridge's highest and lower values were discarded; the remaining data were averaged to determine the asphalt layer thickness. The distance from the surface was measured, the thickness of the paving layer was calculated, and this information was concurrently given to the asphalt paver as they work. The amount of asphalt material released up to the particular paving level may be quickly determined using this approach. Consequently, the NCDS approach offered the following benefits: no direct physical contact with the sublayer beneath the pavement is necessary, which allows for greater flexibility in the paving process; this system also ensures a higher degree of reliability in paving the desired surface layer thickness. However, before the actual paving session, the system had to be calibrated and tested using actual pavement work. A schematic concept of NCDS system and its usage on the Korean expressway network are shown in Figures 5 and 6, respectively.

## 4. Actual Pavement Field Evaluation Sections

The Korean Expressway network's two most recent construction segments were chosen (Table 1 for further details). These field tracks were utilized to compare the NCDS smoothing capabilities against that of the traditional LS + SL method.

About 4,500 km of the Korean expressway system are now under development, with a 90% completion rate [43, 44]. A situation like this is changing the road paving activity from new construction to maintenance techniques heavily focused on asphalt overlay, as for the chosen aged concrete pavement test sections. When current jointed concrete pavements (JCP) reach the end of their useful life, this technique involves adding an asphalt layer on top of them to create a composite pavement system. The advantage of the carefully chosen test section is that NCDS and LS + SL techniques were implemented, enabling a simultaneous comparison. One of the field sections from the building sites used for this experiment is shown in Figure 7.

To evaluate the effectiveness of the NCDS system, a sensor array was attached on each side of the asphalt paver (i.e., left and right side) with a set of three cartridges consisting of five sensors on each side. After removing the extreme (e.g., largest and smallest) thickness values measured from each cartridge of sensors, a total of 18 measurements (i.e., nine values from each side) were acquired for the specific overlaying process. The paving machine's three separate multisonic sensor cartridges were installed at the front, middle, and rear so that, if needed, the sonic waves could be directed both to the already-paved area and to the road shoulder. The pictures in Figure 8 visually presents the position of the sensors of the NCDS system on the asphalt paver.

## 5. Field and Laboratory Testing

*5.1. Asphalt Pavement Surface Smoothness Measurement.* Figure 9 shows the results of three measurements of the IRI value performed at each testing site [45]. It is well known that lower IRI results (and/or trends) indicate smoother pavement surface conditions, providing better car-riding experiences to drivers. The schematic information of IRI measuring equipment is shown in Table 2.

The average values were then obtained, and comparison was performed after removing potential outliers according to the following rules [46] and schematic in Figure 10:

(1) Determine the values of the inter quartile range (IQR) and set Q1 (upper quartile) and Q3 (lower quartile) values.
(2) Calculate the maximum and minimum data range by computing the values of Q3-1.5 * IQR (M3 range) and Q1 + 1.5 * IQR (M1 range).
(3) Identify any measure as an outlier if the measured IRI results are smaller than M3 or higher than M1 values, respectively.

The commercial pavement smoothness analysis application PROVAL (version 3.6) was then used to examine the field data [45, 47]. For each pavement site in the current study, more than 5,000 data were employed for IRI analysis since IRI findings were obtained every 20 cm.

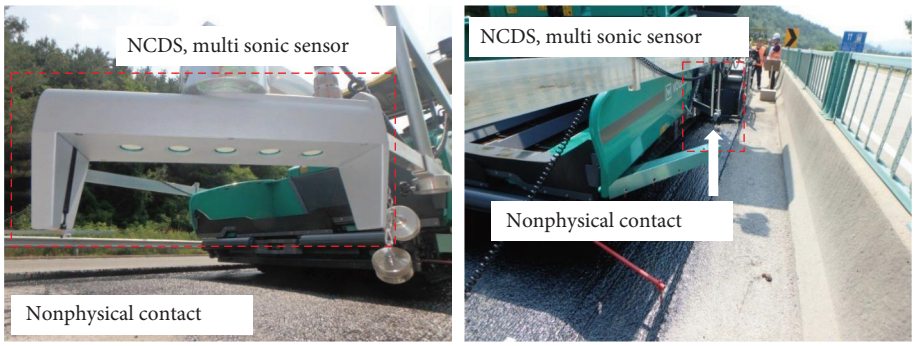


Figure 6: Noncontact digital ski (NCDS) system on a Korean expressway—Ho-Nam expressway, South Korea.

Table 1: South Korea expressway: field sections and sites.

| Expressway (construction date) | Section information | Pavement structure information |
|---|---|---|
| Testing section, No.1<br>(in South Korea)<br>Location: Jun-Nam area<br>Ho-Nam expressway<br>Station: 47.0–48.0 k<br>(2018. July) | Length = 0.80 km<br>(Site A), L = 0.26 km<br>(Site B), L = 0.54 km<br>Lane 1: LS + SL<br>Lane 2: NCDS<br>(width: 3.6 m) | Composite pavement structure<br>Layer 1) Flexible pavement layer<br>SMA, $t = 10$ cm, NMAS: 13 mm<br>(SMA: stone mastic asphalt)<br>(Air void: 2.0–2.8%, Binder: PG 76–22)<br>Layer 2) Rigid pavement layer<br>Concrete (JCP, $t = 30$ cm)<br>(JCP: jointed concrete pavement)<br>(Cement: Ordinary Portland Cement)<br>(Joint location: every 6 m installation)<br>Layer 3) Chemical stabilized layer<br>Cemented layer ($t = 15$ cm)<br>(Consisted of mortar treated layer)<br>Layer 4) Subgrade<br>(Clay soil: upper, Gravel: bottom) |
| Testing section, No. 2<br>(in South Korea)<br>Location: Jun-Nam area<br>Ho-Nam expressway<br>Station: 36.0–37.0 k<br>(2020. August) | Length = 0.47 km<br>(Site C), L = 0.17 km<br>(Site D), L = 0.13 km<br>(Site E), L = 0.17 km<br>Lane 1: LS + SL<br>Lane 2: NCDS<br>(width: 3.6 m) | |

| Layer | Pavement type |
|---|---|
| Layer 1 | Asphalt (SMA, $t = 10$ cm) |
| Layer 2 | Concrete (JCP, $t = 30$ cm) |
| Layer 3 | Cemented layer ($t = 15$ cm) |
| Layer 4 | Subgrade: Soil & Gravel |

NCDS, noncontact digital ski; LS, long-ski; SL, string line.

*5.2. Simple Asphalt Performance Mechanical Test: BBR Mixture Creep Test.* At each of the five locations, sample coring was done together with pavement smoothness evaluation (i.e., IRI, m/km) to provide a preliminary assessment of the response of field mixture as influenced by the paving solution adopted (Table 1 for additional information). Due to the extreme cold on those sites during the winter, a straightforward low-temperature creep test utilizing the BBR was used to assess the material behavior [33–38, 48]. The small size of the BBR samples (i.e., $102.0 \times 12.7 \times 6.25$ mm), which is advantageous for relatively thin layers of asphalt mixture (e.g., $t = 10$ cm), as in the case of an overlay, is the reason for choosing such a test in place of the more popular IDT [33–38, 48, 49]. Therefore, three asphalt mixture cores were collected at each construction site for each paving smoothing technology for a total of 30 asphalt mixture cores. Small beam specimens were cut from this series of samples according to a procedure detailed elsewhere [35–38]. Similar to the testing specification for asphalt binder [33], creep stiffness, $S(t)$, and corresponding $m$-value, $m(t)$, can be easily computed from the results of the midspan deflection, $\delta(t)$ when considering the imposed constant load applied to the specimen (approximately 4,000–6,000 mN) (Equation (1)). Given the higher stiffness commonly experienced on mixtures compared to asphalt binders, the testing duration was extended to 1,000 s, so sufficient time was allocated for observing a meaningful evaluation of the midspan deflection [35–38].

$$S(t) = \frac{1}{D(\mathrm{t})} = \frac{\sigma}{\varepsilon(t)} = \frac{P \cdot l^3}{4 \cdot b \cdot h^3 \cdot \delta(t)}, \quad m(t) = \left| \frac{d\,\mathrm{Log}S(t)}{d\,\mathrm{Log}(t)} \right| \tag{1}$$

where:

$S(t)$: Flexural creep stiffness (" = "MPa)

$D(t)$: Creep compliance (" = "1/MPa)

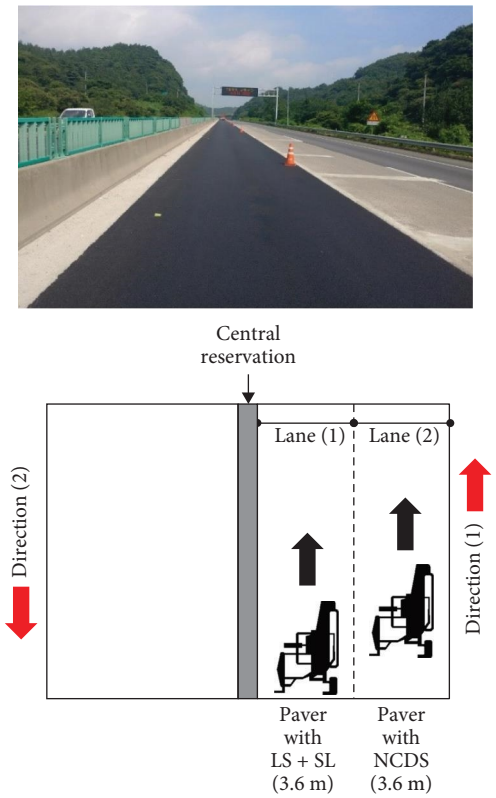


Figure 7: Picture of the testing construction site—Jun-Nam area (conditions at the end of the paving work for Lane 1) Ho-Nam expressway, South Korea.


(a) (b) (c)

Figure 8: NCDS sensors installed on an asphalt paver: (a) front, (b) center, and (c) end.

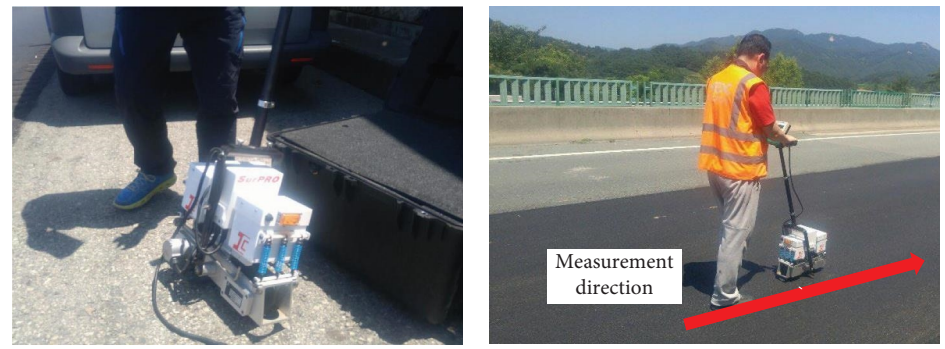


(a) (b)

Figure 9: (a) IRI equipment and (b) IRI measurements.

Table 2: IRI measuring equipment specification.

| Contents | Measuring equipment specification |
|---|---|
| Method | Automated rolling system |
| Sensors | 1 Optical encoder with 1 temperature sensor |
| Measurement reliability | 99.9% repeatability in IRI, medium and long wavelengths |
| Data collect rate | Average: 2 km/hr–Maximum: 4 km/hr |
| Data recording rate | 1 mm |
| Statis resolution | Incline: 0.0019 mm |
| Profile accuracy | +/−2 mm/5 m |
| Weight | 20.4 kg |
| Size | Width: 254 mm * Length: 482 mm |
| Wheel size | Diameter: 152.4 mm * Thickness: 70 mm |
| Computation output | IRI (International Roughness Index), RN (rider number), PI (profilograph index) |
| Data format | Text format (ERD file), ASTM,FHWA (Proval PPF file), Texas DOT (PRO file) and other 10 convertible file formats |

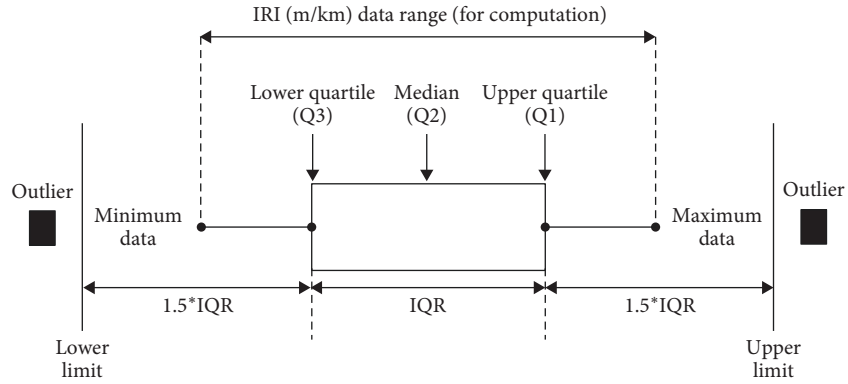


Figure 10: Schematic for the identification of outlier in the IRI (m/km) measurements.

$\sigma$: Bending stress (“=”MPa)
$\varepsilon(t)$: Time-dependent bending strain in the beam
$P$: Applied constant load (“=”mN)
$\delta(t)$: Beam deflection (“=”mm)
$l$, $b$, $h$: Beam dimensions (“=”mm)
$t$: Time (“=”s).

The stone mastic asphalt (SMA) used for the field sections presented a nominal maximum aggregate size (NMAS) of 13 mm and an asphalt binder having performance grade PG 76-22 [34]. Therefore, two temperatures, low (PG + 10°C) and low (PG + 10°C) −12°C (i.e., −22 + 10 = −12°C and −22 + 10 − 12 = −24°C), were adopted for testing and thermal stress estimation, $\sigma(T°C, MPa)$ [35–38]. For each construction site, six replicates were tested per each adopted pavement-smoothing system (i.e., in total 12 BBR beam specimens per each test site: Site A to E). The design of the particular SMA combination adheres to the regulations set out by the South Korean Ministry of Land Infrastructure and Transportation [18]. After the top surface of the pavement was removed, the asphalt mixture samples are shown in Figure 11, and the BBR testing apparatus used in this study is shown in Figure 12.

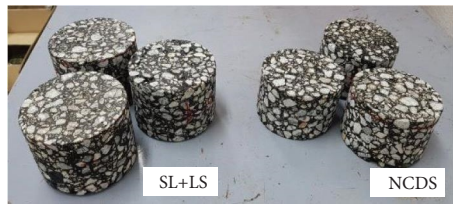


Figure 11: Mixture samples—Site A (SL + LS: string line + long ski, NCDS: noncontact digital ski).

## 6. Computation of Thermal Stress with Advanced Laplace Transformation Approach

Conventionally thermal stress can be computed with complex numerical analysis steps along with Gauss quadrature theory [35–38]. In this paper, an alternative computation method: Laplace transform approach, was selected due to its simplicity with one-step computation process [48, 50–52]. This method consists of a series of steps as detailed below:

(1) Computed the shift factor, $a_T$, from the creep compliance, $D(t)$, at the reference temperature:

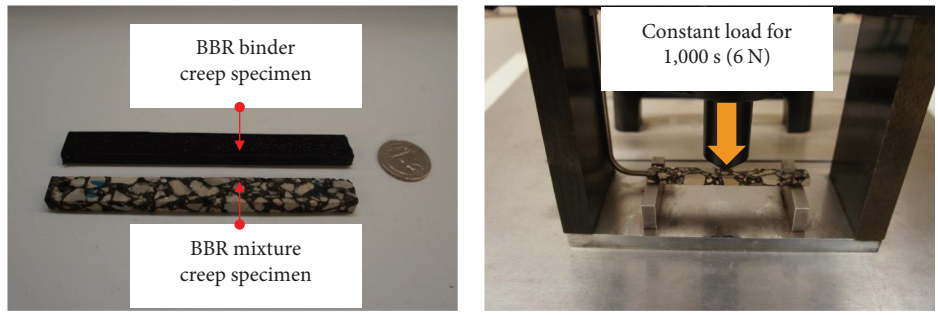


(a) (b)

FIGURE 12: (a) Bending beam rheometer (BBR) test specimens and (b) testing apparatus.

$$a_T = 10^{C_1+C_2\cdot T} = 10^{C_1+C_2\cdot(T_i-C_0\cdot t)} = 10^{(C_1+C_2\cdot T_i)-C_2\cdot C_0\cdot t} = 10^{C_3+C_4\cdot t} = 10^{C_3}\cdot 10^{C_4\cdot t} = A_0\cdot 10^{C_4\cdot t}. \quad (2)$$

(2) Based on the experimental results, obtain the master curve of creep compliance in the reduced time domain, $D(\xi)$, as follows [48, 50–52]:

$$D\left(\xi = \frac{t}{a_T}\right) = A\cdot\left(\frac{t}{a_T}\right)^B + C\cdot\left(\frac{t}{a_T}\right)^D + E \Rightarrow D(\xi) = A\cdot(\xi)^B + C\cdot(\xi)^D + E, \quad (3)$$

where $A$, $B$, $C$, $D$, and $E$ are fitting function parameters. And theses fitting parameters are computed based on experimental asphalt mixture creep compliance: $D$(t), data fitting process.

(3) Apply the Laplace transformation to the conventional equation relating thermal stress to strain:

$$\mathcal{L}(\varepsilon_t) = \mathcal{L}\left(\int_0^\xi D(\xi-\bar{\xi})\cdot\frac{\partial\sigma}{\partial\bar{\xi}}d\bar{\xi} + \int_0^\xi \alpha(\xi-\bar{\xi})\cdot\frac{\partial(\Delta T)}{\partial\bar{\xi}}d\bar{\xi}\right) = s\cdot\overline{D}(s)\cdot\overline{\sigma}(s) + s\cdot\overline{\alpha}(s)\cdot\Delta\overline{T}(s) = 0, \quad (4)$$

where thermal stress and the coefficient of thermal expansion/contraction, $\alpha$, are given by:

$$\overline{\sigma}(s) = -\frac{\overline{\alpha}(s)\cdot\Delta\overline{T}(s)}{\overline{D}(s)}, \quad \alpha(t) = \alpha_0 \Rightarrow \mathcal{L}\alpha(t) = \overline{\alpha}(s) = \frac{\alpha_0}{s}. \quad (5)$$

(4) After performing the inverse Laplace transformation process with the Stephest algorithm [52], $\sigma(\xi)$ can be approximated with a simple power-law function and next converted to the time domain as follows:

$$\sigma(\xi) = A + B\cdot\xi^C + D\cdot\xi^E \text{ and } \xi = A_1\cdot\left(1-10^{-C_4 t}\right), \quad (6)$$

where: $A_0 = 10^{C_3} = 10^{C_1+C_2\cdot T_i}$ and $C_4 = -C_2\cdot C_0$.

Based on this process, $\sigma(T°C)$ can be obtained within the desired temperature range and a 1 mm/s cooling rate. Further details on the computational procedures can be found elsewhere [48, 50–52].

## 7. Field and Laboratory Testing

*7.1. Asphalt Pavement Surface Smoothness Measurement.* All the IRI results are shown in Figures 13–17 and summarized in Table 3. It must be mentioned that IRI measurements were performed three times per each test section (i.e., from Site A to E).

Figures 13–17 report the IRI limit of 1.6 m/km (i.e., solid line parallel to the $x$-axis), which is a quality threshold according to the guidelines of Ministry of Land, Infrastructure and Transport [19, 20]. Lower and uniform IRI (m/km) result trends than 1.6 m/km at each measuring point were observed for the NCDS technology applied section compared to the section paved with LS + SL. Based on the IRI data generation trends, remarkable differences between the two methods can be visually and numerically observed. Approximately 33%–55% higher values of IRI were detected when traditional methods were used (see Table 3). Moreover, when the NCDS system was used, relatively (or remarkably) lower (and/or better) IRI results (e.g., 0.68–1.04 m/km) were observed, suggesting substantial improvements in the asphalt pavement smoothness.

To further support the results of the plots by visual inspection, statistics were used: a hypothesis analysis, $t$-test with a 5% significance level [46] (i.e., $p$-value threshold below which the two smoothing systems can be considered as statistically different). Two assumptions, data normality and constant variance, were imposed [46]. In this paper, a hypothesis test was set as follows:

$$H_{\text{Null}} : \mu_{\text{Group }A:\text{NCDS}} = \mu_{\text{Group }B:\text{LS+SL}}, \quad (7)$$

$$H_{\text{Alternative}} : \mu_{\text{Group }A:\text{NCDS}} \neq \mu_{\text{Group }B:\text{LS+SL}}. \quad (8)$$

In a hypothesis test, Equation (7) means null hypothesis (i.e., mean values: $\mu$ of NCDS and LS + SL, are not significantly different), and Equation (8) presents the alternative hypothesis (i.e., mean values: $\mu$ of NCDS and LS + SL, are significantly different). From Equations (7) and (8), the pooled standard deviation: $S_P$, can be derived as follows:

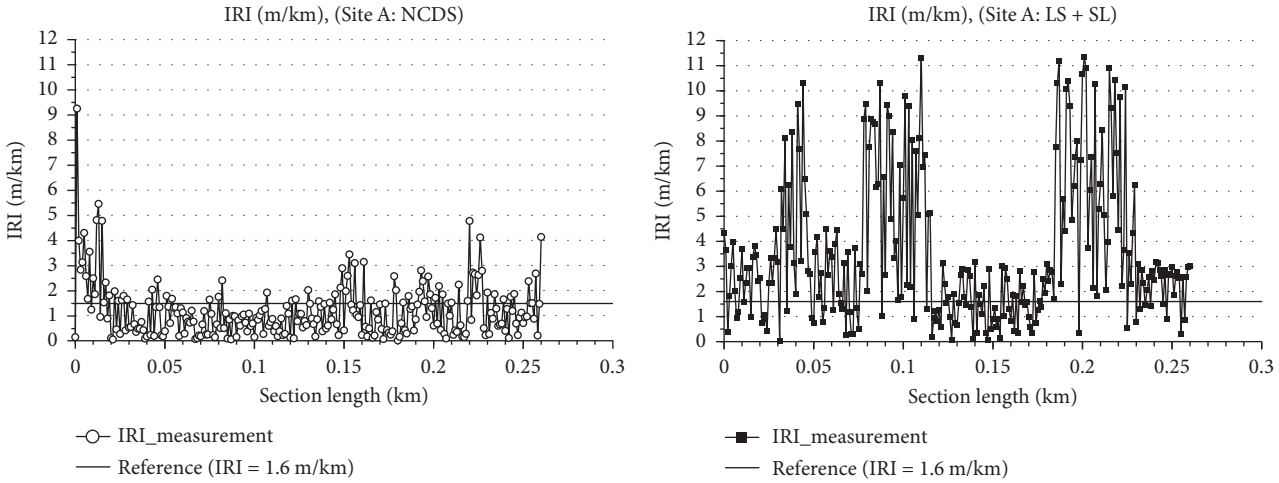


Figure 13: IRI results—Site A ($L = 260$ m): (a) NCDS, (b) LS + SL.

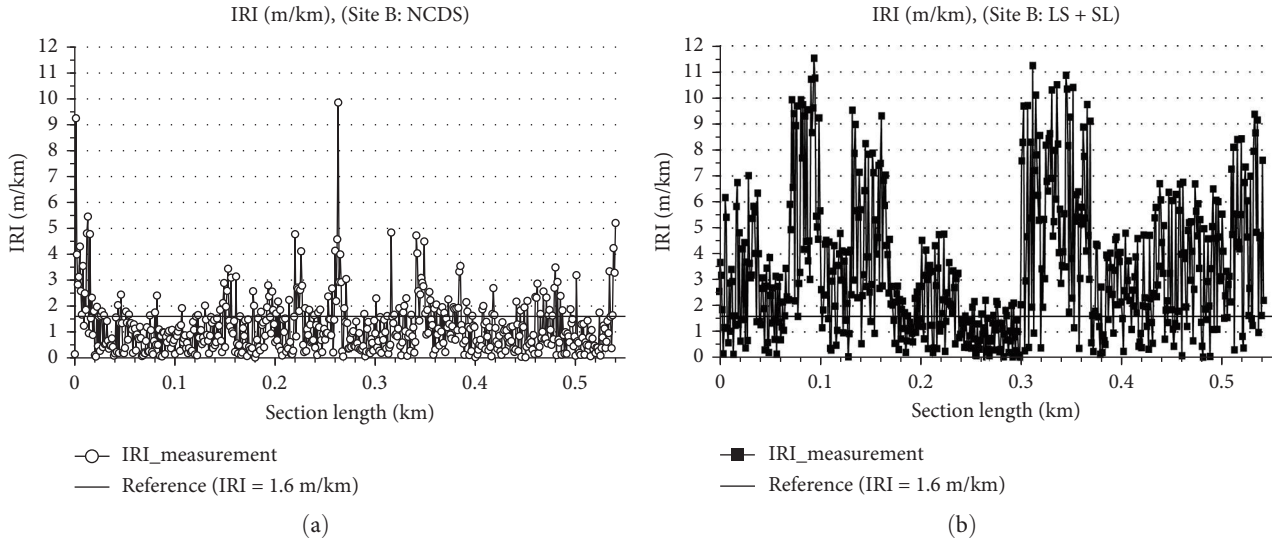


Figure 14: IRI results—Site B ($L = 540$ m): (a) NCDS, (b) LS + SL.

Table 3: IRI (m/km) of the five test sections.

| Site (Length, m) | Averaged results of measured IRI (international roughness index, m/km) (standard deviation) | | |
|---|---|---|---|
| | NCDS (Nonphysical contact) | LS + SL (Physical contact) | Difference (NCDS)–(LS + SL) |
| A ($L = 260$ m) | 1.04 (0.75) | 1.68 (0.96) | 1.04–1.68 = −0.64 (0.64/1.68 = 38%) |
| B ($L = 540$ m) | 1.03 (0.74) | 1.55 (0.94) | 1.03–1.55 = −0.52 (0.52/1.55 = 33%) |
| C ($L = 170$ m) | 0.80 (0.55) | 1.19 (0.72) | 0.80–1.19 = −0.39 (0.39/1.19 = 33%) |
| D ($L = 130$ m) | 0.96 (0.69) | 1.51 (1.31) | 0.96–1.51 = −0.55 (0.55/1.51 = 36%) |
| E ($L = 170$ m) | 0.68 (0.52) | 1.53 (1.02) | 0.68–1.53 = −0.85 (0.85/1.53 = 55%) |

Table 4: Statistical analysis results of IRI (m/km) for the different pavement sites.

| Site | $p$-Value at each length point (significance level, $\alpha = 0.05$) | | | | | | | | |
|---|---|---|---|---|---|---|---|---|---|
| | 10 m | 20 m | 50 m | 100 m | 150 m | 250 m | 350 m | 450 m | 500 m |
| A (260 m) | 1.5e–10 (Sig.) | 2.3e–12 (Sig.) | 1.9e–8 (Sig.) | 4.5e–13 (Sig.) | 5.3e–14 (Sig.) | 6.5e–14 (Sig.) | N/A | N/A | N/A |
| B (540 m) | 2.5e–12 (Sig.) | 2.2e–11 (Sig.) | 1.3e–7 (Sig.) | 2.5e–14 (Sig.) | 4.3e–14 (Sig.) | 1.1e–6 Sig.) | 5.1e–11 (Sig.) | 6.6e–9 (Sig.) | 6.6e–9 (Sig.) |
| C (170 m) | 2.3e–13 (Sig.) | 2.1e–13 (Sig.) | 2.9e–11 (Sig.) | 7.7e–10 (Sig.) | 5.3e–14 (Sig.) | N/A | N/A | N/A | N/A |
| D (130 m) | 1.1e–12 (Sig.) | 1.5e–12 (Sig.) | 4.9e–12 (Sig.) | 8.3e–9 (Sig.) | Non | N/A | N/A | N/A | N/A |
| E (170 m) | 9.5e–6 (Sig.) | 1.8e–13 (Sig.) | 5.9e–9 (Sig.) | 5.1e–10 (Sig.) | 5.3e–14 (Sig.) | N/A | N/A | N/A | N/A |

NCDS, noncontact digital ski; LS, long ski; SL, string line. Sig., statistically significant (significance level $\alpha < 0.05$). N/A, not applicable.

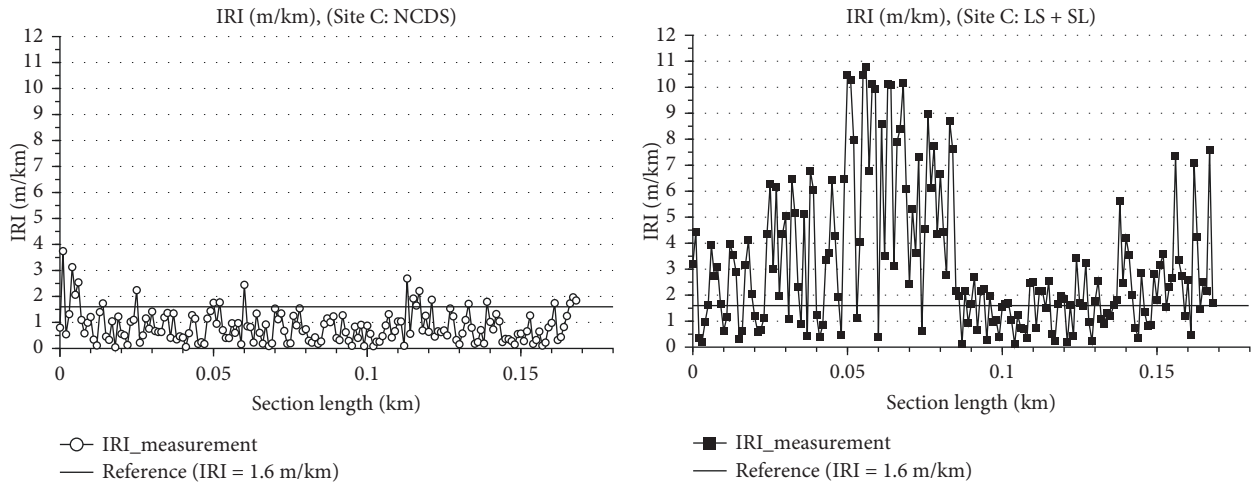


Figure 15: IRI results—Site C ($L = 170$ m): (a) NCDS, (b) LS + SL.

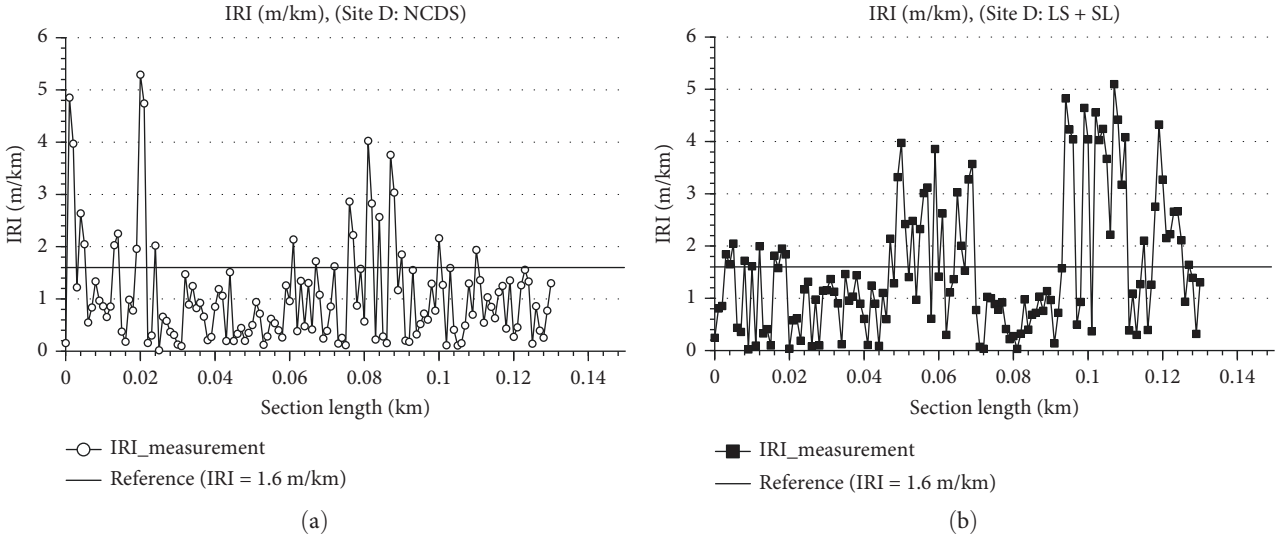


Figure 16: IRI results—Site D ($L = 130$ m): (a) NCDS, (b) LS + SL.

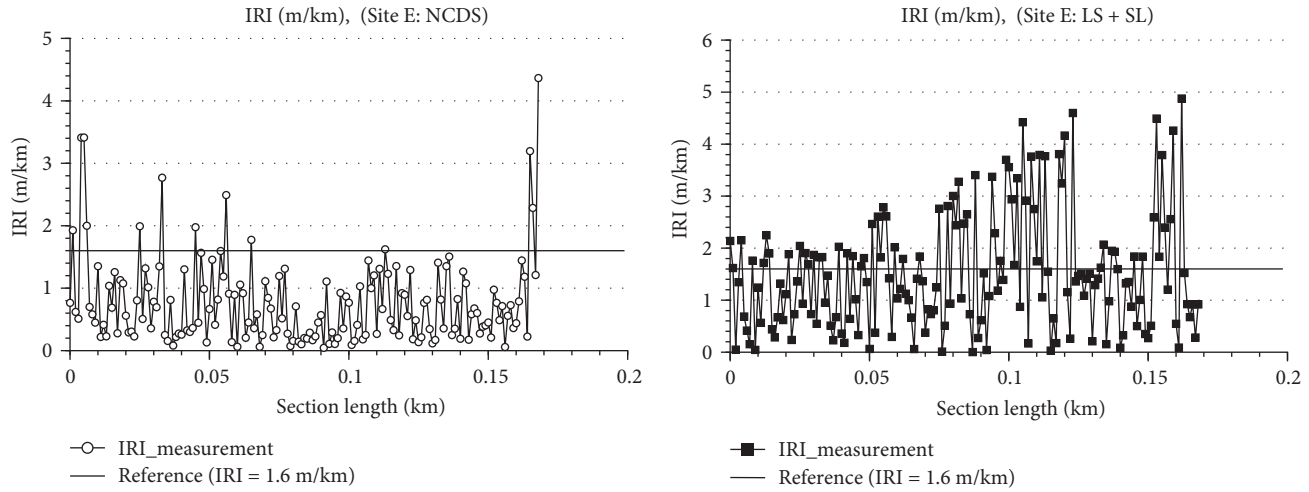


Figure 17: IRI results—Site E ($L = 170$ m): (a) NCDS, (b) LS + SL.

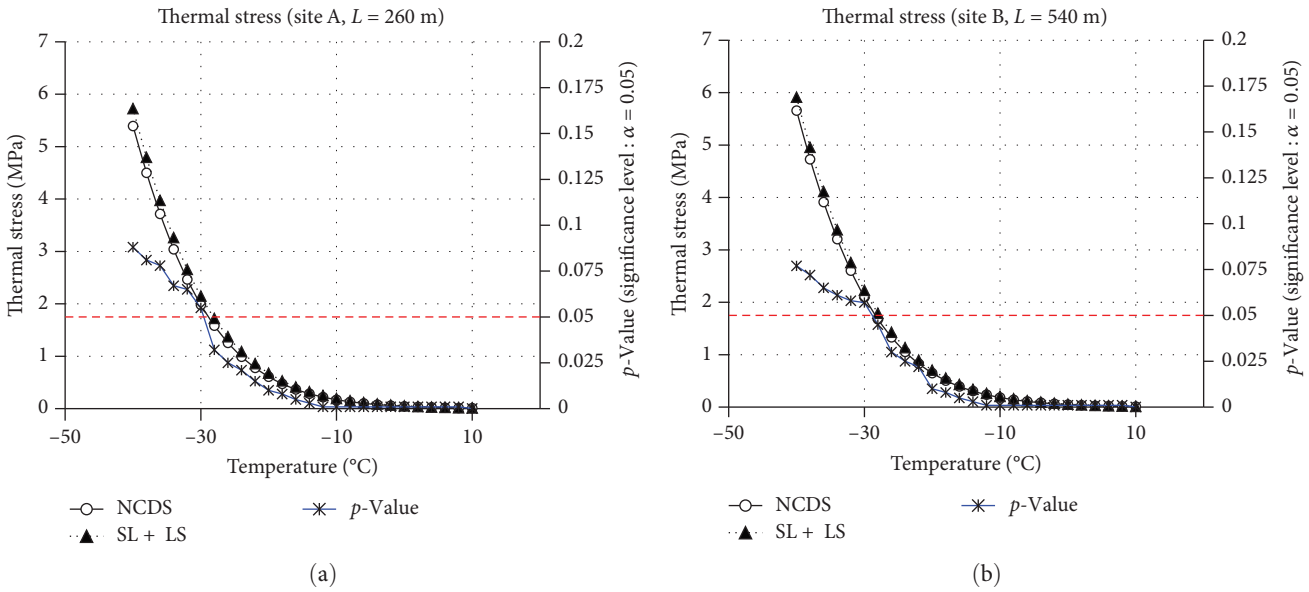


Figure 18: Thermal stress (Site A and Site B).

$$S_P = \sqrt{\frac{(n_A - 1)\cdot S_A^2 + (n_B - 1)\cdot S_B^2}{n_A + n_B - 2}} = \sqrt{\frac{(3-1)\cdot S_A^2 + (3-1)\cdot S_B^2}{3+3-2}} = \sqrt{\frac{2\cdot (S_A^2 + S_B^2)}{4}} = \sqrt{\frac{S_A^2 + S_B^2}{2}}. \quad (9)$$

In Equation (9), $S_A$ and $S_B$ are calculated standard deviation of IRI (m/km) from Group A (i.e., NCDS) and Group B (i.e., LS + SL), respectively. Moreover, $n_A$ and $n_B$ present numbers of IRI (m/km) measurement and evaluation on each test section (e.g., Site A to E).

The results of $t$-static and corresponding degree of freedom: $d_f$, can be derived from Equations (7) to (9) as Equations (10) and (11):

$$t - \text{static} = \frac{|\mu_A - \mu_B|}{S_P \cdot \sqrt{\frac{1}{n_A} + \frac{1}{n_B}}} = \frac{|\mu_A - \mu_B|}{S_P \cdot \sqrt{\frac{1}{3} + \frac{1}{3}}} = \frac{|\mu_A - \mu_B|}{S_P \cdot \sqrt{\frac{2}{3}}} = \frac{|\mu_A - \mu_B|}{\sqrt{\frac{(n_A-1)\cdot S_A^2 + (n_B-1)\cdot S_B^2}{n_A+n_B-2}} \cdot \sqrt{\frac{2}{3}}} = \frac{|\mu_A - \mu_B|}{\sqrt{\frac{(3-1)\cdot S_A^2 + (3-1)\cdot S_B^2}{3+3-2}} \cdot \sqrt{\frac{2}{3}}} = \frac{|\mu_A - \mu_B|}{\sqrt{\frac{2\cdot (S_A^2 + S_B^2)}{4}} \cdot \sqrt{\frac{2}{3}}} = \frac{|\mu_A - \mu_B|}{\sqrt{\frac{(S_A^2 + S_B^2)}{3}}}, \quad (10)$$

$$d_f = n_A + n_B - 2 = 3 + 3 - 2 = 4. \quad (11)$$

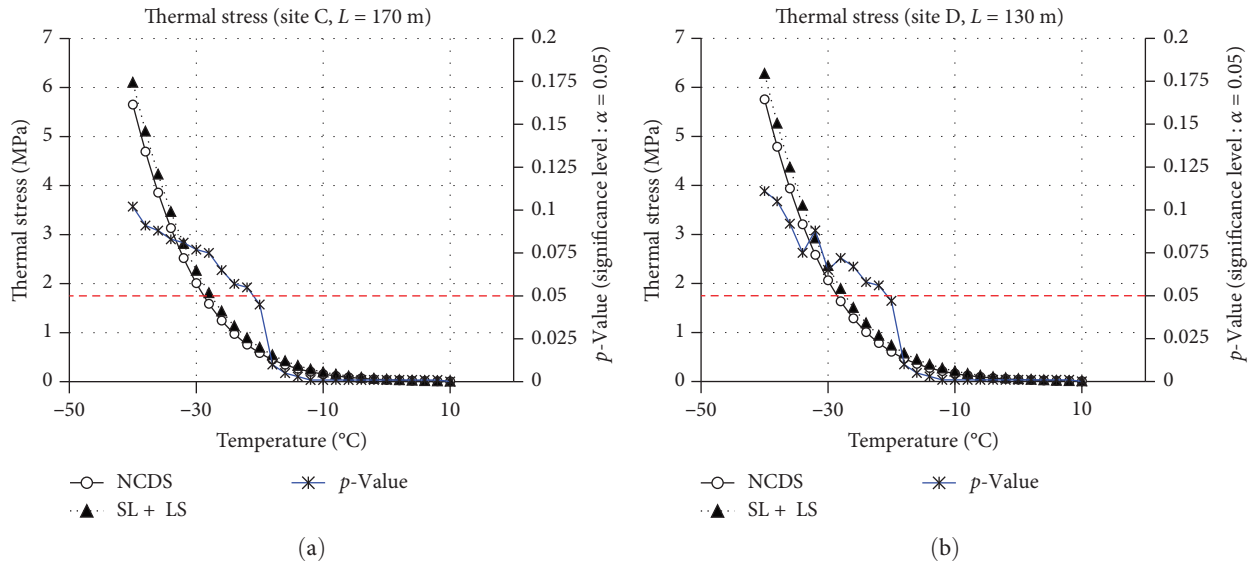


Figure 19: Thermal stress (Site C and Site D).

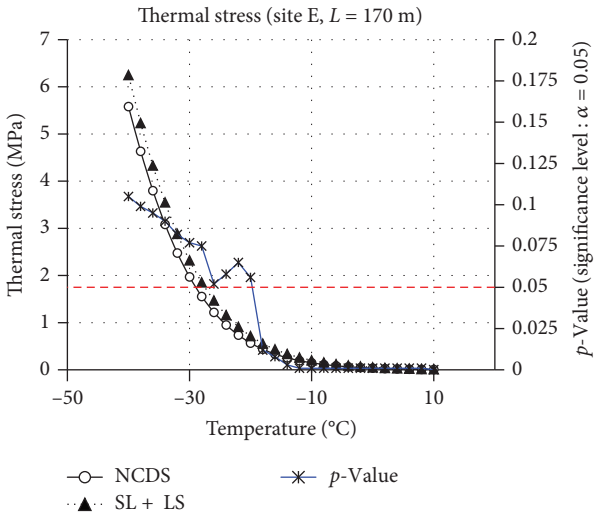


Figure 20: Thermal stress (Site E).

More details on how to conduct this analysis can be found in the literature [46]. The final output of the statistical analysis is summarized in Table 4 in terms of $p$-value with 5% of significant level (i.e., $\alpha = 0.05$). If the results of $p$-value are higher than 0.05, the null hypothesis is accepted (i.e., Equation (7)); otherwise, the alternative hypothesis (i.e., Equation (8)) is accepted.

It is possible to notice significant variations in IRI (m/km) between NCDS and LS + SL. When the LS + SL system was used, greater IRI (m/km) values were discovered on all of the tested sections, which might be the reason for a possibly worse driving experience. This finding implies that the NCDS method may significantly improve pavement evenness and smoothness, even when weighing the advantages against the time needed for initial calibration.

*7.2. Low-Temperature Cracking Resistance Comparison (NCDS vs. LS + SL).* In this section, thermal stress: $\sigma$ ($T$°C), results of cored asphalt mixture specimens were compared through visual and statistical analysis approaches. Thermal stress: $\sigma$ ($T$°C), results were computed based on the previous section (Section 6, Equations (2)–(6)). The calculated thermal stress results are presented in Figures 18–20. Moreover, the statistical comparison process was also performed for $\sigma$ ($T$°C) with a $t$-test; the results were incorporated in the same series of plots. The statistical analysis (i.e., hypothesis test) was performed based on Equations (7)–(10) with values of $n_A$ and $n_B$ corresponding to 6, respectively.

The thermal stress plots demonstrate that for all five test sites, the NCDS technique was shown to provide relatively lower thermal stress levels than the traditional SL + LS smoothing technology. Below −20°C, which is near the PG limit of the asphalt binder employed in the SMA mix design formula, statistical analysis shows no significant differences between the SL + LS and NCDS techniques. But when the temperature dropped below −20°C (Sites C, D, and E) or −30°C (Sites A and B), clear differences could be seen. This suggests that the smoothing system had a moderate impact on the asphalt material's rheological and mechanical response in addition to its surface characteristics, with the use of the NCDS device showing potentially positive behavior.

## 8. Summary and Conclusions

In this study, the viability of using the NCDS, a next-generation asphalt pavement surface smoothing technology, was assessed and contrasted with the traditional approach used to build South Korea's primary expressway asphalt road network. The nonphysical interaction between the smoothing apparatus and the pavement layer and the real-time optimized pavement thickness calculating system are the NCDS system's main advantages over conventional techniques. The following two keypoints can be highlighted:

(1) It was discovered that applying the NCDS technique led to noticeably decreased IRI as supported by the measurements at different filed sites.

(2) When NCDS was used, relatively lower thermal stress values from the field mixture were detected, perhaps indicating greater performance against low-temperature cracking resistance with added advantages.

Based on the findings, remarkable improvements in smoothing asphalt pavement surfaces can reasonably be expected utilizing NCDS technology application. However, it needs to be remarked that equipment calibration (i.e., in the paving construction site or on a test section) is essentially required before the actual pavement construction can be performed with the NCDS tool.

## 9. Recommendations

In this work, just a short pavement portion was taken into account. To further confirm the incredibly optimistic results of this article, longer pavement test sections (for example, more than 4 km long) with different asphalt compositions are required. The first findings of this combined field and laboratory study are encouraging and support further study into the application of the NCDS system for paving. This is a component of ongoing research that also includes a nondestructive pavement performance assessment, a larger laboratory testing campaign, and an expanded selection of combinations for asphalt overlay.

## Data Availability

The data results in this paper are available only with the permission of the corresponding author.

## Conflicts of Interest

There are no conflicts of interest in this paper.

## Acknowledgments

The access to the testing sections and the experimental support provided by the Korea Expressway Corporation Pavement Research Division (KECPRD) are warmly acknowledged by the authors.

## References

[1] B. Choubane, R. L. McNamara, and G. C. Page, "Evaluation of high-speed profilers for measurement of asphalt pavement smoothness in Florida," *Transportation Research Record: Journal of the Transportation Research Board*, vol. 1813, no. 1, pp. 62–67, 2002.

[2] K. L. Smith, L. Titus-Glover, and L. D. Evans, *Pavement Smoothness Index Relationships*, Federal Highway Administration (office of pavement technology), United States (U.S.), Final report (No. FHWA-RD-02-057), 2002.

[3] H. H. Titi and M. Rasoulian, "Evaluation of smoothness of Louisiana pavements based on international roughness index and ride number," *Jordan Journal of Civil Engineering*, vol. 2, no. 3, pp. 238–249, 2008.

[4] A. Bae, D. Lee, and J. Y. Tan, "IRI reduction of HMA overlay on concrete base slab in urban tunnel expressway," in *Transportation Research Board 94th Annual Meeting*, Article ID 12, TRID, 2015.

[5] A. Bae, D. Lee, and J. Y. Tan, "Smoothness improvement by HMA overlay on very rough surface in urban tunnel expressway," *KSCE Journal of Civil Engineering*, vol. 21, pp. 2177–2185, 2017.

[6] A. Bae, H.-S. Lee, and D.-J. Jung, "Paver sensor system performances on the initial smoothness of HMA pavement," *International Journal of Highway Engineering*, vol. 20, no. 5, pp. 13–21, 2018.

[7] Y. Yildirim and G. Saygili, "Pavement smoothness of asphalt concrete overlays," *International Journal of Pavement Engineering*, vol. 20, no. 1, pp. 73–78, 2019.

[8] F. Guo, J. Pei, G. Huang, Z. Hu, Z. Niu, and A. C. Falchetto, "Evolution of tire-pavement friction with the regular surface macro-texture characteristics and environmental factors using 3D printing technology," *Journal of Cleaner Production*, vol. 382, Article ID 135293, 2023.

[9] B. Smith, "Factors affecting the IRI of asphalt overlays," in *Transportation Research Board 93rd Annual Meeting*, Article ID 18, TRID, 2014.

[10] J. J. Hajek, T. J. Kazmierowski, and D. K. Hein, "The effect of increased initial smoothness on pavement performance," in *The 5th Symposium on Pavement Surface Characteristics of Roads And Airports*, Article ID 10, TRID, Toronto, Ontario, Canada, 2004.

[11] K. K. McGhee and J. S. Gillespie, "Value of pavement smoothness," *Transportation Research Record: Journal of the Transportation Research Board*, vol. 2040, no. 1, pp. 48–54, 2007.

[12] I. Zaabar and K. Chatti, "Estimating vehicle operating costs caused by pavement surface conditions," *Transportation Research Record: Journal of the Transportation Research Board*, vol. 2455, no. 1, pp. 63–76, 2014.

[13] M. M. Robbins and N. H. Tran, "A synthesis report: value of pavement smoothness and ride quality to roadway users and the impact of pavement roughness on vehicle operating costs," , National Center For Asphalt, Auburn University, Auburn, Alabama, Technology report 16-03, 2016.

[14] K. Park, N. E. Thomas, and K. W. Lee, "Applicability of the international roughness index as a predictor of asphalt pavement condition," *Journal of Transportation Engineering*, vol. 133, no. 12, pp. 706–709, 2007.

[15] H. Ziari, J. Sobhani, J. Ayoubinejad, and T. Hartmann, "Prediction of IRI in short and long terms for flexible pavements: ANN and GMDH methods," *International Journal of Pavement Engineering*, vol. 17, no. 9, pp. 776–788, 2016.

[16] T. D. Gillespie, M. W. Sayers, and L. Segel, "Calibration of response type road roughness measuring systems," National Cooperative Highway Research Program report (No. 228), 1980.

[17] M. W. Sayers, T. D. Gillespie, and W. D. O. Paterson, "Guidelines for the conduct and calibration of road roughness measurements," , The World BanK, Washington, DC, USA, World Bank Technical Paper No. 46, 1986.

[18] M. W. Sayers, T. D. Gillespie, and C. A. V. Queiroz, "International road roughness experiment: establishing methods for correlation and a calibration standard for measurements," , World Bank Group, Washington, DC, World Bank Technical Paper (No. 45), 1986.

[19] "MOLIT: Guideline for production and construction of asphalt mixture (specification. ministry of land infrastructure and transportation (in Korean)," 2017.

[20] "MOLIT: Road practice manual. ministry of land infrastructure and transportation (in Korean)," 2019.

[21] R. W. Perera and S. D. Kohn, "LTPP data analysis: factors affecting pavement smoothness," Transportation Research

Board, National Cooperative Highway Research Program (web document 40), 2001.
[22] C. M. Raymond, S. L. Tighe, R. Hass, and L. Rothenburg, "Analysis of influences on as-built pavement roughness in asphalt overlays," *International Journal of Pavement Engineering*, vol. 4, no. 4, pp. 181–192, 2003.
[23] P. Lu and D. Tolliver, "Pavement treatment short-term effectiveness in IRI change using long-term pavement program data," *Journal of Transportation Engineering*, vol. 138, no. 11, pp. 1297–1302, 2012.
[24] Q. Dong and B. Huang, "Evaluation of effectiveness and cost-effectiveness of asphalt pavement rehabilitations utilizing LTPP data," *Journal of Transportation Engineering*, vol. 138, no. 6, pp. 681–689, 2012.
[25] F. Dalla Rosa, L. Liu, and N. G. Gharaibeh, "IRI prediction model for use in network-level pavement management systems," *Journal of Transportation Engineering, Part B: Pavements*, vol. 143, no. 1, Article ID 04017001, 2017.
[26] M. Mubaraki, "Third-order polynomial equations of municipal urban low-volume pavement for the most common distress types," *International Journal of Pavement Engineering*, vol. 15, no. 4, pp. 303–308, 2014.
[27] M. Mubaraki and H. Sallam, "The most effective index for pavement amangement of urban major roads at a network level," *Arabian Journal for Science and Engineering*, vol. 46, pp. 4615–4626, 2021.
[28] H. Gong, Y. Sun, X. Shu, and B. Huang, "Use of random forests regression for predicting IRI of asphalt pavements," *Construction and Building Materials*, vol. 189, pp. 890–897, 2018.
[29] N. Li, R. Qin, and Z. Liu, "Performance measures and evaluation of asphalt pavements using the internal roughness index," in *Pavement and Geotechnical Engineering for Transportation*, pp. 19–30, ASCE Library, March 2013.
[30] N. M. H. Elagamy, "*An experimental and numerical study of three-dimensional fatigue damage in carbon fiber reinforced polymers*," Doctoral Dissertation, Carleton University, 2016.
[31] "Writgen group: big multiplex ski (product information)," 2022, https://www.wirtgen-group.com/en-us/.
[32] "MOBA group: Sensor product information," 2022, https://moba-parts.com/sensors/.
[33] AASHTO, *Standard Method of Test for Determining the Flexural Creep Stiffness of Asphalt Binder Using the Bending Beam Rheometer (BBR) (Specification T313-12)*, American Association of State Highway and Transportation Officials, Washington, DC, 2012.
[34] AASHTO, *Standard Specification for Superpave Volumetric Mix Design (Specification M323)*, American Association of State Highway and Transportation Officials, Washington, DC, 2017.
[35] M. Marasteanu, R. Velasquez, and A. Cannone Falchetto, *Development of a Simple Test to Determine the Low Temperature Creep Compliance of Asphalt Mixture*, Transportation Research Board, Washington, DC, USA, 2009.
[36] K. H. Moon, "*Comparison of thermal stresses calculated from asphalt binder and asphalt mixture creep compliance data*," M. S. thesis, University of Minnesota Digital Conservancy, 2010.
[37] K. H. Moon, "*Investigation of asphalt binder and asphalt mixture low temperature properties using analogical models*," Ph.D. thesis, University of Minnesota Digital Conservancy, 2012.
[38] K. H. Moon, A. C. Falchetto, M. Marasteanu, and M. Turos, "Using recycled asphalt materials as an alternative material source in asphalt pavements," *KSCE Journal of Civil Engineering*, vol. 18, pp. 149–159, 2014.
[39] A. Al-Qudsi, A. C. Falchetto, D. Wang, S. Büchler, Y. S. Kim, and M. P. Wistuba, "Finite element cohesive fracture modeling of asphalt mixture based on the semi-circular bending (SCB) test and self-affine fractal cracks at low temperatures," *Cold Regions Science and Technology*, vol. 169, Article ID 102916, 2020.
[40] C. Riccardi, I. Indacoechea, D. Wang, P. Lastra-González, A. C. Falchetto, and D. Castro-Fresno, "Low temperature performances of fiber-reinforced asphalt mixtures for surface, binder and base layer," *Cold Regions Science and Technology*, vol. 206, Article ID 103738, 2023.
[41] C. Riccardi, A. C. Falchetto, and D. Wang, "Three-dimensional characterization of asphalt mixture containing recycled asphalt pavement," *Asphalt Paving Technology: Association of Asphalt Paving Technologists-Proceedings of the Technical Sessions*, vol. 89, pp. 75–94, 2021.
[42] D. Wang, A. C. Falchetto, C. Riccardi, and M. P. Wistuba, "Investigation on the low temperature properties of asphalt binder: glass transition temperature and modulus shift factor," *Construction and Building Materials*, vol. 245, Article ID 118351, 2020.
[43] K. H. Moon, T. S. Yoo, J. C. Kim, and J. S. Park, "An application study on selecting proper and optimized sections for remodeling of aged pavement," , Korea Expressway Corporation (KEC, in Korean), Final research report (KECRI-2017-32-534.9607), 2017.
[44] D.-H. Kim, J.-M. Lee, K.-H. Moon, J.-S. Park, Y.-C. Suh, and J.-H. Jeong, "Development of remodeling index model to predict the priority of large-scale repair works of deteriorated expressway concrete pavements in Korea," *KSCE Journal of Civil Engineering*, vol. 23, pp. 2096–2107, 2019.
[45] "International cybernetics: product manual-SurPRO (SurPRO-4000/5000 model series)," 2022.
[46] D. R. Cook and S. Weisberg, *Applied Regression Including Computing and Graphics*, John Wiley & Sons, Inc, New York, 1999.
[47] "The transtec group: software manual-proval: version 3.6," 2021, http://www.roadprofile.com.
[48] K. H. Moon, O. S. Kwon, M. J. Cho, and F. A. Cannone, "An alternative one-step computation approach for computing thermal stress of asphalt mixture: the Laplace transform," *KSCE Journal of Civil and Environmental Engineering Research*, vol. 39, no. 1, pp. 219–225, 2019.
[49] AASHTO, *Standard Method of Test for Determining the Creep Compliance and Strength of Hot Mix Asphalt Using the Indirect Tensile Test Device*, American Association of State Highway and Transportation Officials, Washington, DC, (Specification T322-07), 2007.
[50] A. C. Falchetto and K. H. Moon, "An alternative method for computing thermal stress in asphalt mixture: the Laplace transformation," *Road Materials and Pavement Design*, vol. 18, no. Sup2, pp. 226–240, 2017.
[51] A. C. Falchetto, K. H. Moon, and D. H. Kim, "Evaluation of recycled asphalt mixture at low temperature using different analytical solutions," *Canadian Journal of Civil Engineering*, vol. 47, no. 7, pp. 801–811, 2020.
[52] H. Stehfest, "Algorithm 368: numerical inversion of Laplace transform," *Communication of the Association for Computing Machinery (ACM)*, vol. 13, pp. 47–49, 1970.